Toughness of HDPE/$CaCO_3$ Microcomposites Prepared from Masterbatch by Melt Blend Method

Ilias Ali,[1,2] Rabeh Elleithy[1]

[1]*SABIC Polymer Research Center (SPRC), King Saud University, Riyadh 11421, Saudi Arabia*
[2]*Chemical Engineering Department, King Saud University, Riyadh 11421, Saudi Arabia*

Received 13 October 2010; accepted 21 February 2011
DOI 10.1002/app.34417
Published online 12 July 2011 in Wiley Online Library (wileyonlinelibrary.com).

ABSTRACT: In this study, a series of high-density polyethylene and micro/nanocalcium carbonate polymer composites (HDPE/$CaCO_3$ nanocomposites) were prepared via melt blend technique using a twin screw extruder. Nanocomposite samples were prepared via injection molding for further testing. The effect of % loading of $CaCO_3$ on mechanical and fracture toughness of these composites has been investigated in details. The effect of precrack length variation on the fracture toughness of the composite samples was evaluated, and the morphology of the fractured samples was also observed using scanning electron microscopy (SEM). It was found that increasing the % of $CaCO_3$ and precrack length decreased the fracture toughness. Fracture surface examination by SEM indicated that the diminished fracture properties in the composites were caused by the aglomerization of $CaCO_3$ particles which acted as stress concentrators. A finite element analysis using ANSYS was also carried out to understand the effect of agglomeration size, interaction between the particles and crack tip length on the fracture properties of these composites. Finally, a schematic presentation of the envisioned fracture processes was proposed. © 2011 Wiley Periodicals, Inc. J Appl Polym Sci 122: 3303–3315, 2011

Key words: tensile; fracture; toughness; microscopy; nano; $CaCO_3$; masterbatch; HDPE; composite

INTRODUCTION

Recently, polymer nanocomposites are in the limelight as a new generation materials because of their advantages and unique properties synergistically derived from nanoscale structure displaying enhanced physical, mechanical, thermal, electrical, magnetic, and optical properties.[1] Further, these benefits can be achieved even at very low concentration of the nanofillers in comparison to conventional polymer composites.[2] Therefore, it is important to develop practical and economical solutions and processing methods for tailoring of sustainable materials configurations at the nanoscale level. Recently, much progress has been made in meeting these challenges and in developing a wide range of commercial process, products, and devices as a result of the research efforts and advances by many scientist, engineers, and technologist.[3] Modification of the strength and toughness of semicrystalline polymers is always a subject of intense researcher. A direct relation between molecular characteristics and macroscopic mechanical properties of polymeric materials is attracted by vast number academic and industrial researcher. High-density polyethylene (HDPE), a semicrystalline polyolefin which is one of the most used thermoplastic materials as commodity plastics due to its low price, balanced properties and easy processability, however because of its low toughness, weather resistance, and environmental stress cracking resistance which have limited its application in many technologically important areas.[4]

A wide varieties of reinforcing agents, such as calcium carbonate ($CaCO_3$), mica, wollastonite, glass fiber, glass bead, jute, curaua fiber, silica (SiO_2), clay, CNT, etc., are being used to prepare polymer composites/nanocomposites.[5–9] Calcium carbonate ($CaCO_3$) is one of the most widely used minerals in polyolefin composite industry because of its low cost and abundance, and moreover it is available globally in a variety of particle sizes (macro to nano), shapes, and purities.[10–13] The effect of addition of nanosized calcium carbonate with polyethylene on physical properties has been investigated extensively.[14]

The improvement of toughness of thermoplastic nanocomposite is also an important area of research. Giannelis et al.[15] reported the toughening mechanism of polyvinylidene fluoride (PVDF) and polyactide-*co*-glycolide (PLG) layered silicate nanocomposites.[16] Sivaramana et al.[17] reported the fracture toughness of thermoplastic copoly (ether ester) elastomer and ABS blends. Liu et al.[18] showed the improvement of fracture toughness of immiscible polypropylene/ethylene-*co*-vinyl acetate blends with

Correspondence to: Rabeh Elleithy (rhelleithy@yahoo.com).

© 2011 Wiley Periodicals, Inc.

multiwalled carbon nanotubees. Toughness mechanism in semicrystalline polymer such as high-density polyethylene toughened with rubbers has also been reported.[19] Thermoplastics filled with fillers showed a significant decrease of fracture toughness compared to the neat polymer matrix.[20,21] There are, however, several studies that show toughness increase with introduction of inorganic fillers in PP and PE.[22] Impressively enhanced impact toughness has been reported for polyethylene filled with calcium carbonate particles by Fu and Wang[23–25] and Bartczak et al.[26] Toughness mechanism in semicrystalline high-density polyethylene toughened with calcium carbonate has also been published.[27] The mechanical properties of hybrid composites are dictated not only by their composition, but also by their phase morphology. A limited numbers of studies were being carried out to correlate the morphology with the toughness behavior of HDPE-$CaCO_3$ composites.

With the current growth in the automotive market, part molders are demanding more process-able materials to meet the increasing demand of these composites. In the context of industrial applications, melt blending is the preferred method of composite preparation. Melt blending using masterbatch is one of the simplest, economical, and environmental-friendly methods in processing of plastic composites. A few reports are available in the literature for the preparation of a composite by masterbatch approach.[28–30] Therefore, the masterbatch containing micro/nanofillers approach to prepare HDPE composites seems to be attractive and ecofriendly.

In this communication, we report fracture toughness of HDPE/$CaCO_3$ composite having different $CaCO_3$ loading prepared by melt blend method from a masterbatch. The effect of the % loading of $CaCO_3$ masterbatch and precrack length on the fracture toughness of these composite is also reported. The fracture toughness of these composite with morphology is also investigated and an attempt has been made to understand the mechanism of fracture in these composites. A finite element analysis using ANSYS 12.1 was also carried out to understand the particle size, interaction between the particles and crack tip length on the fracture properties of these composites.

MATERIALS AND METHODS

Materials

High-density polyethylene (HDPE-54; melt index of 30 g/10 min, density of 0.954 g/cm^3, and tensile strength @ yield of 1200 MPa) from a local Saudi manufacturer was used in this work. It is an injection molding grade of HDPE copolymer with a narrow molecular weight distribution and high flowability. Calcium carbonate $CaCO_3$ Filler-0189 which is a masterbatch granules of LLDPE as a carrier and an equivalent $CaCO_3$ content of approximately 80% ± 3% in the masterbatch. The $CaCO_3$ size is 20 nm to 2 μm, and the melt flow index is ≤3.0 g/10 min. The masterbatch is supplied by Wuxi Changhong Masterbatches, China. The masterbatch conformed to health and safety standards of the European Resolution AP 89.[1]

TABLE I
List of the Samples Used in this Work

Sample	Description
NC-0	HDPE-54 + 0% $CaCO_3$ filler masterbatch
NC-10	HDPE-54 + 10% $CaCO_3$ filler masterbatch
NC-20	HDPE-54 + 20% $CaCO_3$ filler masterbatch

Compounding

HDPE was premixed with different ratio of $CaCO_3$ masterbatch. The $CaCO_3$ masterbatch ratio was varied from 10 to 20%. Subsequently, the premix was pelletized using an intermeshing and corotating twin screw extruder, Farrell FTX20. The premix was dried in a conventional oven at 80°C for 5 h before processing. The screw diameter was 26 mm, and the L/D ratio was 35. The screw had both dispersive and distributive mixing elements. The screw speed was 15 rpm and the temperature profile used (from feed to die) was 180, 230, 235, 240, 240, 235, and 240°C. The melt pressure was about 6 bar during the processing of these composites. The extrudate was cooled in water bath at about 25°C, air dried, and pelletized for further use. One control material from neat HDPE-54 and two different composites were prepared as listed in Table I. Thereafter, ASTM specimens were molded from the previously prepared pellets for further analysis.

Some of the thermal properties of pellets of NC-0, NC-10, and NC-20 samples are listed in Table II.[26]

Injection molding

An injection molding machine (Asian Plastic Machinery, Double Toggle IM Machine, Super Master Series SM 120) was used to mold ASTM standard samples. The molding conditions are listed in Table III. The molded specimens were conditioned at 23°C for 24 h before further testing.

TABLE II
Some of the Physical Properties of the Sample Used in this Work

Sample	T_m (°C)[a]	X_r[a]	MFI g/10 min (at 190°C)
NC-0	131	1.00	36
NC-10	132	0.89 ± 0.6	30
NC-20	132	0.87 ± 0.6	28

[a] Relative polymer crystallinity calculated from DSC measurements.

TABLE III
Details of Injection Conditions

Injection molding conditions					
Temperature profile (°C)				Cool time (s)	Water circulation temperature (°C)
Die zone	Zone III	Zone II	Feed zone	15	10-11
210	230	220	160		

Tensile test and fracture toughness

The tensile response of the dumbbell-shaped specimens, ASTM D638, of the samples were studied at room temperature, using a Hounsfield H100 KS series tensile testing machine. The tensile tests were performed at different crosshead speed of 50, 100, and 500 mm/min.

The single edge notched (SEN) specimen for the fracture toughness measurements were prepared by inducing a precrack to one side of the ASTM tensile sample with a sharp thin razor blade (Fig. 1). The precrack length was varied from 10 to 60% (% of a/D). Different SEN specimens were prepared as described and tested for their fracture toughness. All of the reported measurements for all of the tests in this research represent the median of three experiments.

Fractography

A scanning electron microscope, SEM, (JSM 6360A, JEOL) was used to study the fracture surface of the tensile and single edge notch samples. The surfaces of the samples were coated with a thin layer of gold under vacuum prior to the SEM observation to avoid electrostatic charging and heat build-up during examination.

Finite element analysis

To envision the effect of incorporation of the $CaCO_3$ particles on the fracture process, a finite element model was constructed using ANSYS 12.1 finite element analysis (FEA) software. For the model, it was assumed that interfacial bonding between the HDPE and $CaCO_3$ is weak and also that the particles to be incompressible voids in HDPE matrix around which a stress concentration is induced on loading. It was also assumed that the shapes of the particles were either spherical or elliptical. Moreover, we assumed that the particles were evenly distributed through the polymer matrix.

RESULTS AND DISCUSSION

Tensile strength

The relationship between the stress and strain of HDPE-54 and its composites are shown in Figure 2. The stress–strain curve could be divided into six regions: (i) elastic deformation, (ii) plastic deformation, (iii) yielding, (iv) necking, (v) neck-spreading, then (vi) fracture as shown in the inset of Figure 2.

The characteristic property of the elastic region is Young's modulus which is a measure of the "stiffness" of the material. As the loading of $CaCO_3$ increased, Young's modulus increased as shown in Figure 3 where the stiffening effect of $CaCO_3$ on HDPE-54 is clearly observed. This increase in the stiffness is about 50% at $CaCO_3$ loading of 20%. That is to say, for the same stiffness, the cross section of identical parts made of NC-20 could be thinner that that made of NC-0. This could be translated to a saving of material used to make identical parts from NC-20 as opposed to NC-0.

Figure 2 shows that yield stress decreases with increasing the % loading of $CaCO_3$. In our previous work,[31] we showed that $CaCO_3$ agglomerates in samples of composites with higher $CaCO_3$ loading. Visual observation of deforming specimens of the composites samples showed that yield and plastic

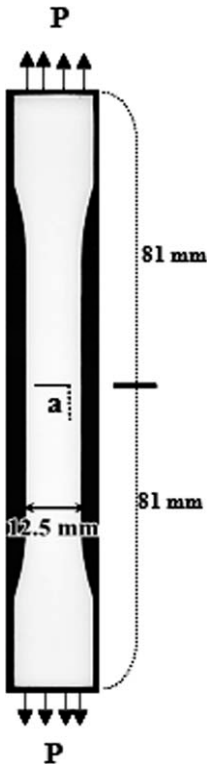

Figure 1 Specimen geometry showing precrack for the toughness measurements. (*a*: precrack length; *D*: width of the sample; and *P*: applied stress).

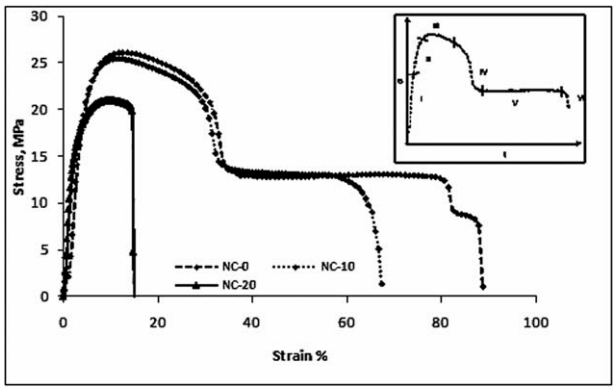

Figure 2 Stress–strain profile of neat HDPE (NC-0) and HDPE/$CaCO_3$ composites samples (NC-10 and NC-20).

flow is accompanied by very strong whitening of the sample in the necking zone for all compositions with $CaCO_3$. This suggested extensive "crazing" that could result from debonding of the particles from the matrix occurring near the yield point. This debonding confirms a state of low adhesion between $CaCO_3$ and HDPE polymer matrix as was seen from morphological analysis.[32] Debonding is especially important in polyethylene (PE) composites because of low polarity and low free energy of polymer. Interfacial adhesion is weak and separation of matrix–filler interface can happen rapidly.[33] Not only did the strength of the composites decreased, but also their ductility was reduced as well where the samples fractured shortly after the yield as seen from Figure 2. A comparison of ultimate elongation (Fig. 4) of the blends and neat HDPE demonstrates that fillers induced a definite decrease in elongation to fracture that becomes very substantial for composite samples with 20% $CaCO_3$ materbatch loading as shown in Figure 4.

Strain rate sensitivity

Figure 5 shows the relation of tensile strength and the different extensional speed, for composite samples

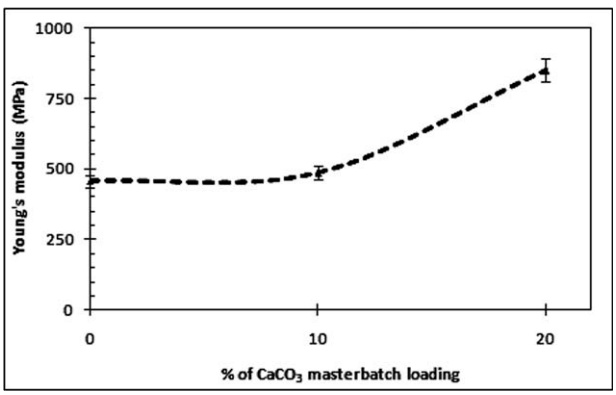

Figure 3 Variation of modulus with % $CaCO_3$ masterbatch loading.

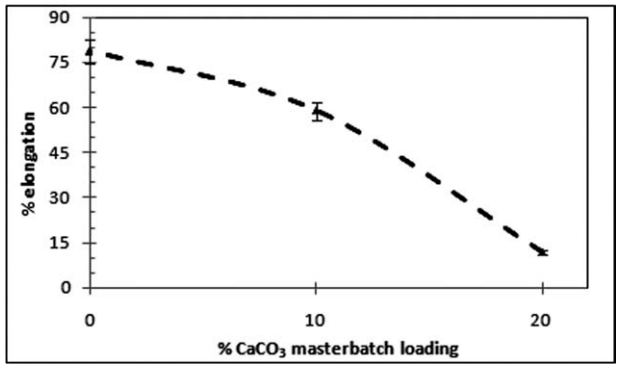

Figure 4 Variation of elongation at break with % $CaCO_3$ masterbatch loading.

with different $CaCO_3$ loadings. It was observed that at any testing speed, tensile stress decreased as $CaCO_3$ loading increased. This could be due to the fact that $CaCO_3$ acted as a stress concentrator. Therefore, as the loading of $CaCO_3$ increased, the stress concentration increased, and hence strength decreased.[34]

Fracture toughness

Fracture toughness of polymers and composites is a crucial property that is often neglected. It is so detrimental as it describes the resistance of material to crack propagation. The highest the fracture toughness, the more resistance the material is to crack propagation. The fracture toughness (K_I) of the neat HDPE-54 resin (NC-0) and the composite samples NC-10 and NC-20 were calculated according to eq. (i) using single-edge notch (SEN) samples under tension. Equation (ii) can also be used to calculate the fracture toughness that considers the geometric correction factor (Y^2). The value of geometric corrections factors (Y^2) are shown in Table IV.[35]

$$K_I = \sigma\sqrt{\pi a} \quad \text{(i)}$$

$$K_I^2 = Y_{(a/D)}^2 \sigma^2 a \quad \text{(ii)}$$

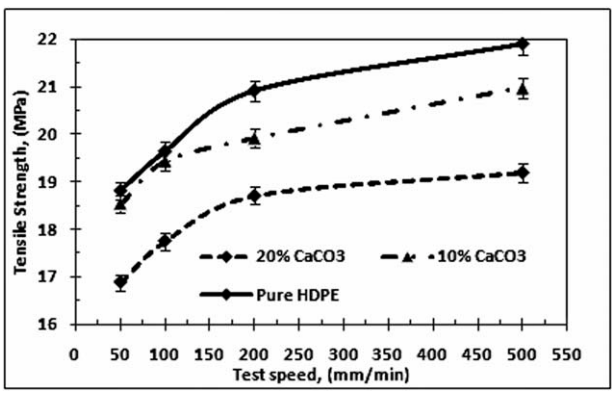

Figure 5 Tensile strength of HDPE and its nanocomposite at different strain rate.

TABLE IV
Finite with Correction Factor

a/D	Y^2 (SEN)
0.1	4.42
0.2	5.92
0.4	13.94
0.6	51.03

Where K_I is the fracture toughness, σ is stress at break, a is precrack length, and D is the width of the sample tested.

Figure 6 represents the variation of K_I of HDPE-54 and composites samples with $CaCO_3$ containing masterbatch content. As seen, the addition of 10 and 20% of $CaCO_3$ masterbatch loading to neat HDPE decreases its fracture toughness (K_I). Compared to the neat HDPE-54 the fracture toughness of the composite samples decreased by about 50%. Similarly Zabardi et al.[36] reported 37% reduction of fracture toughness of HDPE $CaCO_3$ nanocomposite at a similar $CaCO_3$ loading. In other words, addition of $CaCO_3$ led the composites samples toward brittle behavior. These stress concentrators increased the localized stresses around the debonded particles as depicted in the finite element analysis in Figure 7. Moreover, agglomerization is well-known phenomenon in $CaCO_3$,[32] and the tendency of the nano/micro $CaCO_3$ to agglomerate increased the effect of the stress concentration where bigger debonding area has higher stresses than the small ones as shown in Figure 7. In addition, our earlier publication[31,32] we showed that there are larger size $CaCO_3$ for higher loadings of $CaCO_3$ than that of smaller

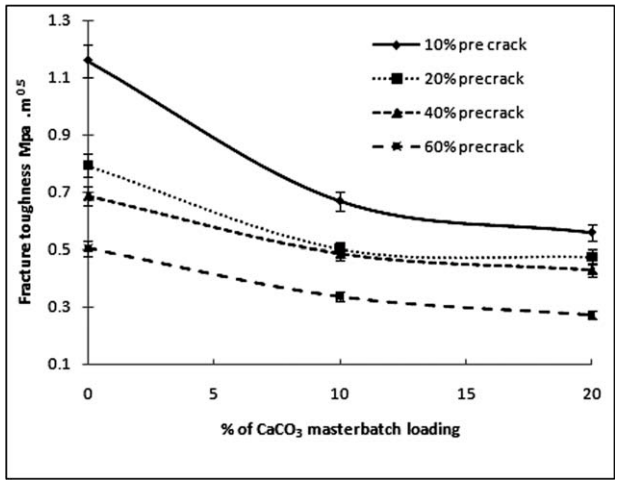

Figure 6 Variation of fracture toughness with % $CaCO_3$ masterbatch loading.

loading. We also observed that the processing condition employed for the preparation of these composite was not enough to break the agglomerization at higher % loading of $CaCO_3$. Moreover, the masterbatch did not have any agent to prevent agglomeration of $CaCO_3$. Thus, the particles aggregate act like a big single particle. Aggregation is explained by the tendency of the nanoparticles to decrease their surface contact with matrix by agglomeration. Uncoated $CaCO_3$ particles tend to aggregate and, as mentioned earlier, the agglomerated particles acted as stress concentrator points, hence reducing the fracture toughness and promote brittle fracture.[36–39] Moreover, from the morphological investigation of the fracture samples it was evident that there is no or

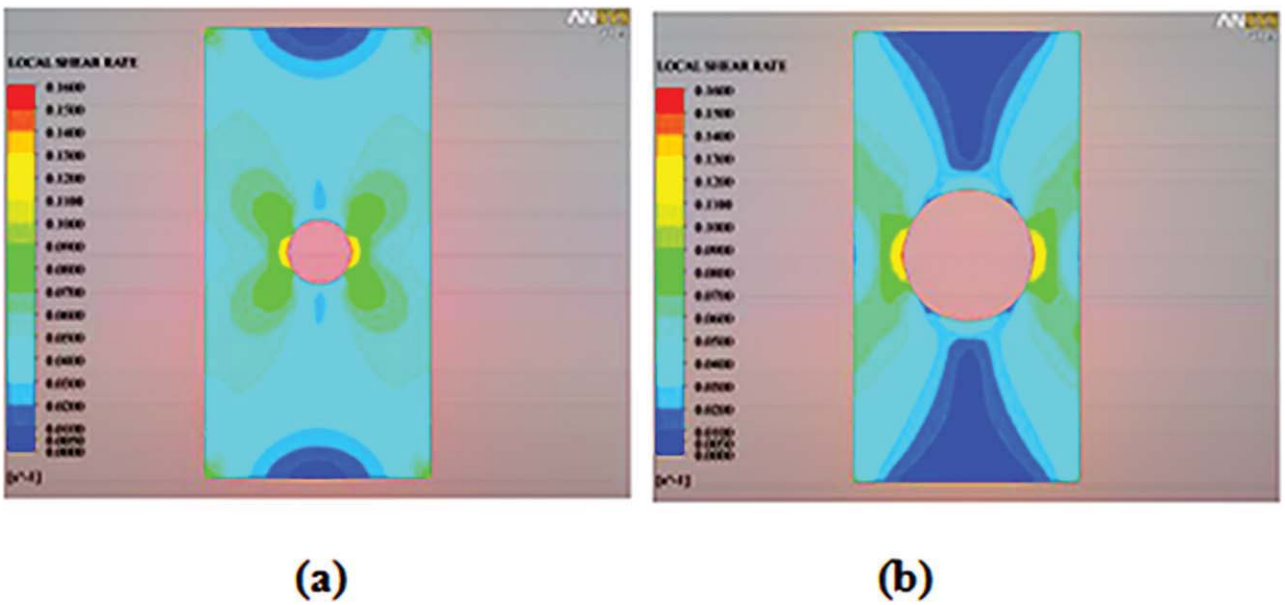

Figure 7 Simulation of stress concentration (a) for small particles and (b) bigger/agglomerated particles by ANSYS 12.1. [Color figure can be viewed in the online issue, which is available at wileyonlinelibrary.com]

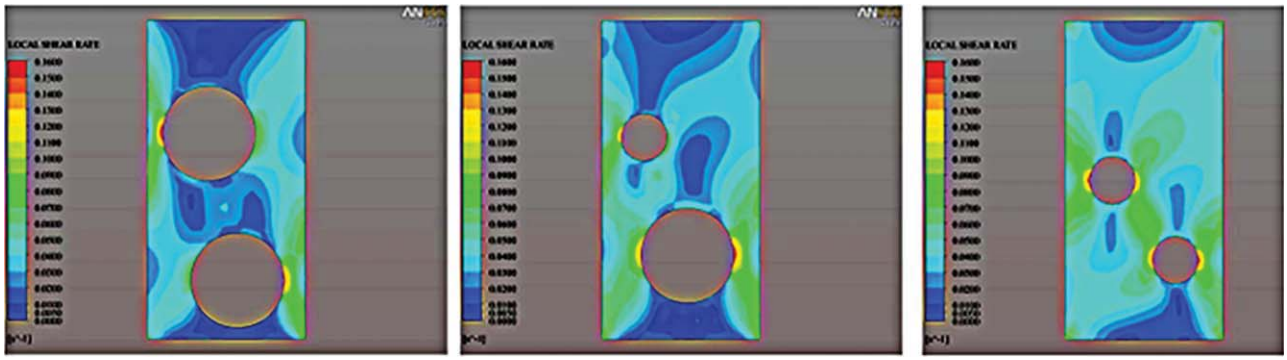

Figure 8 ANSYS simulation showing the interaction between different sized the particles. [Color figure can be viewed in the online issue, which is available at wileyonlinelibrary.com]

little adhesion between the $CaCO_3$ particles and the HDPE polymer matrix. Since the filler/matrix interface is not strong enough thus deformation of the matrix interface is not the dominated energy absorption mechanism but rather debonding is suggested to be the controlling mechanism.

The fracture energy could be consumed by interface debonding, crack initiation, and propagation. It is worth noting that the debonding energy is decreased with increasing the particle size,[38] which could lead to the decrease of fracture toughness as particle size increased. Other investigators reported that the main part of the fracture energy is consumed by matrix deformation and a little part of the energy could be consumed via debonding.[35] In addition, crack can propagate through interface easily because of the weak interface. Moreover, as the $CaCO_3$ content increases, there is a better chance of particles interaction as shown in Figure 8. Particles interactions would generate larger areas that have higher stresses than other areas of the polymer matrix. These areas of higher stresses act as possible crack initiation zones.

Also, particles are not necessarily round, perpendicular elliptical particles [Fig. 9(a)] generate more stress concentration at their poles than those aligned parallel to the stress axis [Fig. 9(b)]. All of the abovementioned discussed reasons could explain why did the fracture toughness decreases with increasing calcium carbonate content. A probable mechanism of fracture is also discussed in the morphological investigation part.

Figure 10 shows the dependency of the K_I on the precrack length. As the precrack length increased the fracture toughness decreased. The decrease is believed to be due to the change of the fracture mechanism from a mix of ductile/brittle, to one that is predominantly brittle. This change of fracture mechanism is due to the induced effect of stress concentration as % of $CaCO_3$ increased as explained earlier.

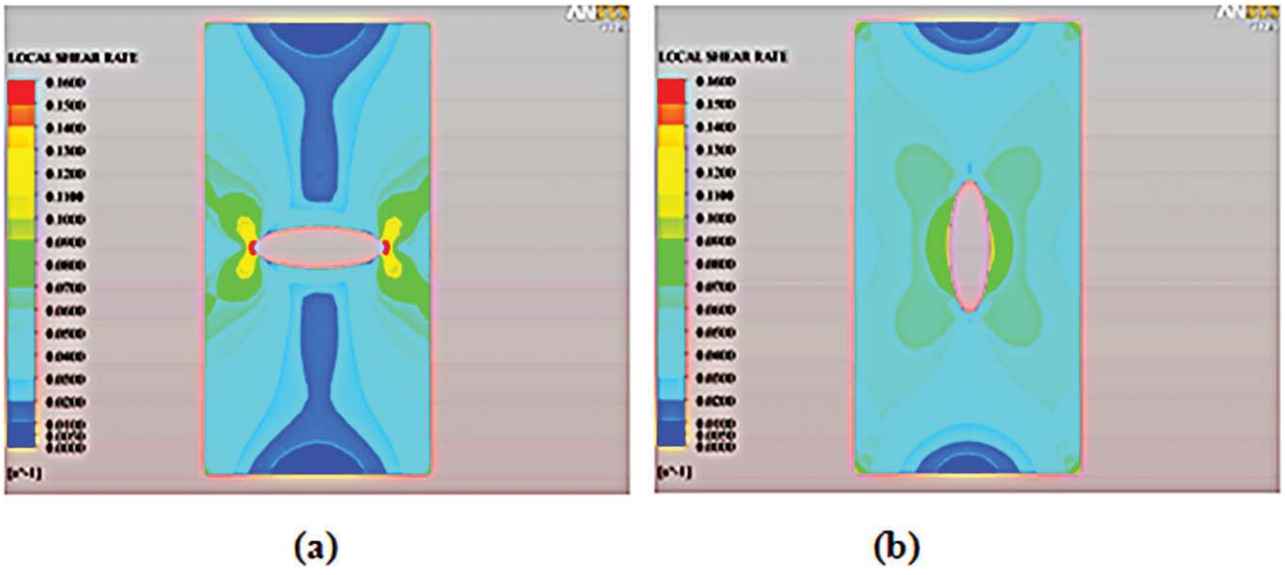

Figure 9 ANSYS simulation showing the effect of void orientation on induced stress. [Color figure can be viewed in the online issue, which is available at wileyonlinelibrary.com]

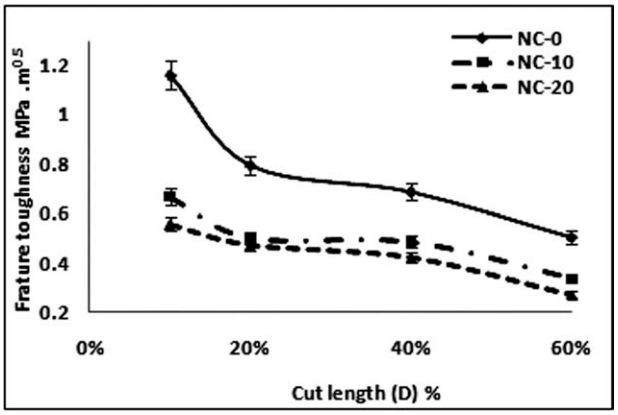

Figure 10 Variation of fracture toughness with % precrack length.

Figure 11 shows the induces stresses in front of a crack for different crack lengths by FEA method. From this analysis, it is clearly evident the stress is more in the sample where precrack length is highest. Hence K_I decreased as cut length increases.

The fracture toughness reported in the present communication is slightly different from the values reported by other authors. One explanation is that the fracture toughness can be affected by molecular weight and crystallinity structure of the matrix polymer.[41] Hence not all HDPE would behave in the same fashion as these could have different molecular weight and crystallinity. For example, Li et al.[42] observed a rise in fracture toughness as molecular weight increase and fracture toughness depends on spherulite size also. While spherulite diameter increases a decrease in fracture toughness can be observed. However, this effect will be negligible as molecular weight increases.

Fractography of tensile samples

For NC-0 when fractured at a cross head speed of 500 mm/s without any precrack, the fracture surface showed a ductile fracture features where the matrix had the characteristic dimples that developed into fibrils. The micrographs of Figure 12 shows the fractured surfaces of HDPE and composites which display an interchange of multiple crazing/voiding then developing of dimples fibrillation of the matrix. All of the tensile samples showed characteristic ductile fracture morphology. However, the level of ductility decreased as the percentage of $CaCO_3$ increased as indicated by the fibril lengths and width. The fibril length of NC-0 was found to be longer than that of NC-20. For NC-20 composite sample, the full development of dimple to fibrillate was restricted which in turn reduced the composites ductility as compared to the neat resin.

Fractography of SEN samples

Microscopic investigation of the fracture surfaces of NC-0, NC-10, and NC-20 samples with a precrack revealed a completely different morphology and fracture mechanism than that of the tensile sample. A general schematic representation of the fracture samples with a precrack is shown in Figure 13.

The surface of fractured sample with a precrack can be divided into three main zones: I, initial precrack; II, slow crack propagation zone; and IV, fast crack propagation zone. In addition, the crack propagation zone could be further subdivided into three zones, namely, transition zone III (slow-to-fast propagation zone) and two skin zones V and VI. The slow crack propagation zone (II) has an elliptical shape that could be characterized by its length (L) and width (d).

From the fractographic investigation of the fracture surface of sample NC-0 (Fig. 14), it is clearly visible that the sample fractured via both ductile and brittle fracture mode. The micrograph is divided into different zones according to the scheme as described in Figure 13. The mechanism of fracture is primarily dominated by the length of the precrack (a/D). The samples with precrack length of 10 and 20% fractured through both ductile/brittle fracture

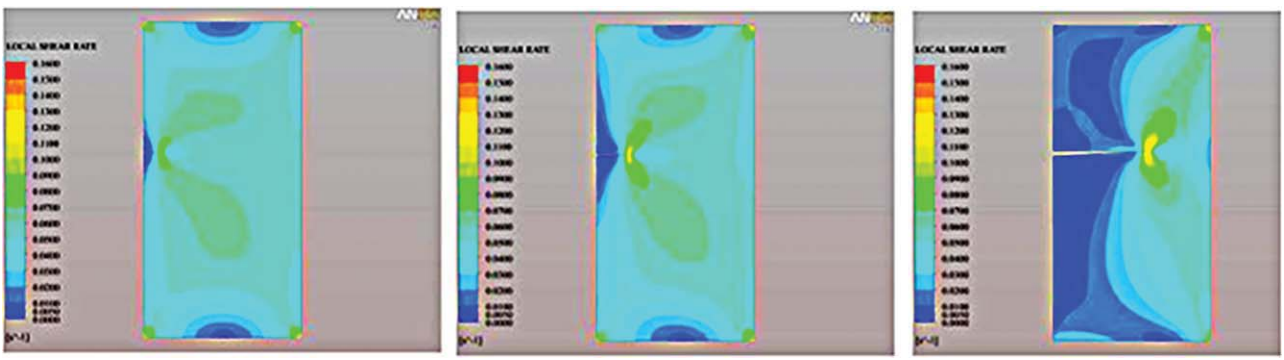

Figure 11 ANSYS simulation showing the dissipation and process zones in front of a crack for the different crack length by FEA method. [Color figure can be viewed in the online issue, which is available at wileyonlinelibrary.com]

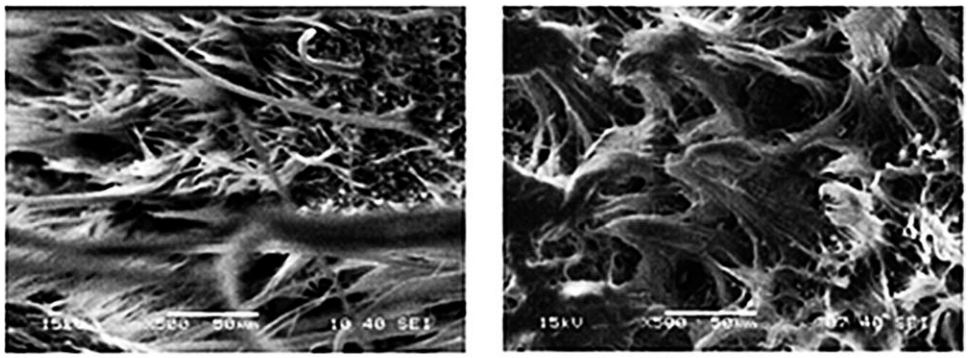

Figure 12 SEM micrographs of fractured tensile samples of (a) NC-0 and (b) NC-20 without a precrack.

mode. Although samples with precrack length of 40 and 60% fractured mostly by a brittle fracture mode, and the brittle fracture was truncated. There was a distinctive effect of the precrack length on the Zones II and IV (Fig. 13). As the crack length increased the length of Zone IV decreased as well. In samples with 10 and 20% precrack length, the length of Zone II and Zone IV were almost equal, but in samples with 40 and 60% precrack length, the length of Zone II was found to be highest. It was also observed that the characteristic parabolic crack propagation pattern was more developed in the samples with pre crack length of 10 and 20%, whereas parabolic shape became more elongated, i.e., *L* increased, for the precrack length of 40 and 60%. Moreover, it was also observed that the crack propagated in Zone-II had some island like voids/cracks as shown in Figure 15. In addition, fibrillation of HDPE matrix was clearly observed in slow propagation zone (Zone-II). These observed fibrils were parallel to the direction of crack propagation, indicating an intense plastic deformation process. Previous studies have demonstrated that these fibrils can effectively slow down the propagation of the local craze and then improve the dissipation of external stress by enhancing the local plastic deformation of the HDPE matrix.[9,28] From the SEM investigation, it can be concluded that the precrack length dictated the fracture morphology and mechanism of fracture in this study. It is worth mentioning that we did not observe any stick-slip type propagation during the crack deformation in the neat HDPE polymeric matrix. Other authors, Misra et al.[40,42] reported that the stick-slip crack propagation was associated with the dynamic crack propagation effects which occurred when the crack momentarily stopped when its speed was below a critical value. This indicated that the crack speed in our case was always above its critical value.

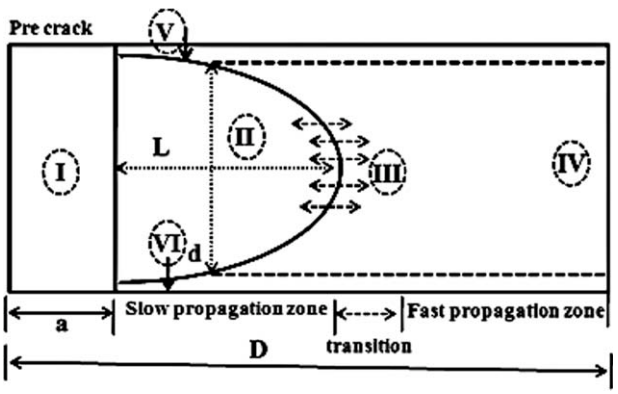

Figure 13 Schematic representation of fracture surface of HDPE or composite with a precrack.

For HDPE/$CaCO_3$ composite samples (NC-20), as shown in Figure 16, the fracture surface can be divided into similar zones as described for neat HDPE samples NC-0 (Fig. 14). The overall macroscopic fracture surface displayed more brittle characteristics than that of the neat resin. It was evident from the fractographic investigations that the mechanism of fracture is dominated by the brittle fracture mode. There is distinctive effect of the precrack length on Zone-II (L) and Zone -IV as observed earlier in NC-0. As the crack length increased the length of Zone-II increased and length of Zone-IV decreased. It was also observed that the HDPE fibril became thinner at higher $CaCO_3$ loading and at higher magnification and debonding of the $CaCO_3$ is clearly visible (Fig. 17). In the sample with precrack length 60% the slow propagation zone is more than the fast propagation zone. At higher magnifications of the fast propagation zone, we observed no fibrillation and formation of voids is also observed around the $CaCO_3$ particles (Fig. 17). It was also observed that the characteristics parabolic crack propagation pattern is not developed in the samples as observed in the NC-0 sample with all precrack length (Fig. 18). However, the propagation pattern is more elongated in the samples with 60% precrack length. Moreover, it was also observed that the crack propagated in Zone-II had island like voids/cracks as observed in

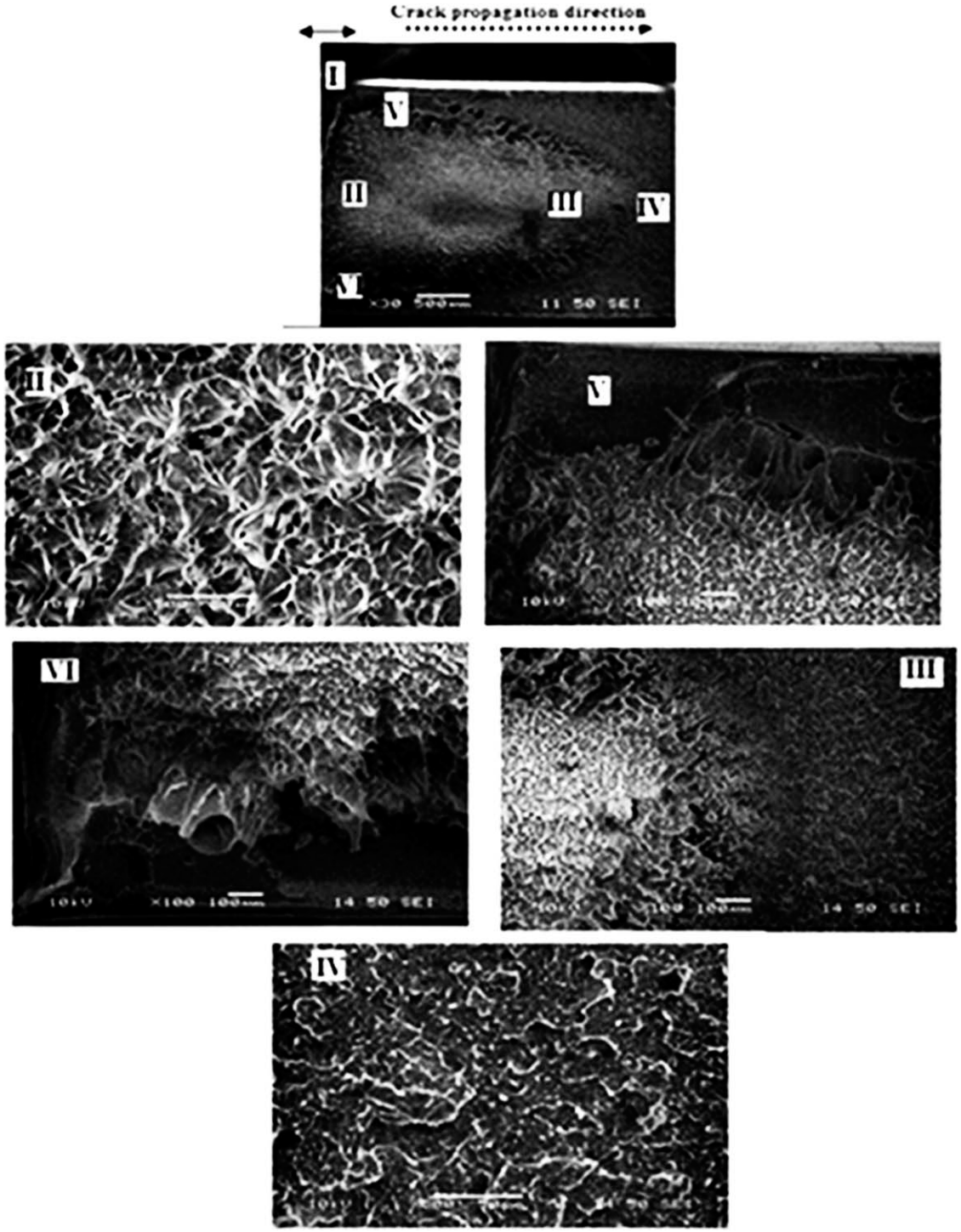

Figure 14 SEM micrographs of NC-0 showing different zones.

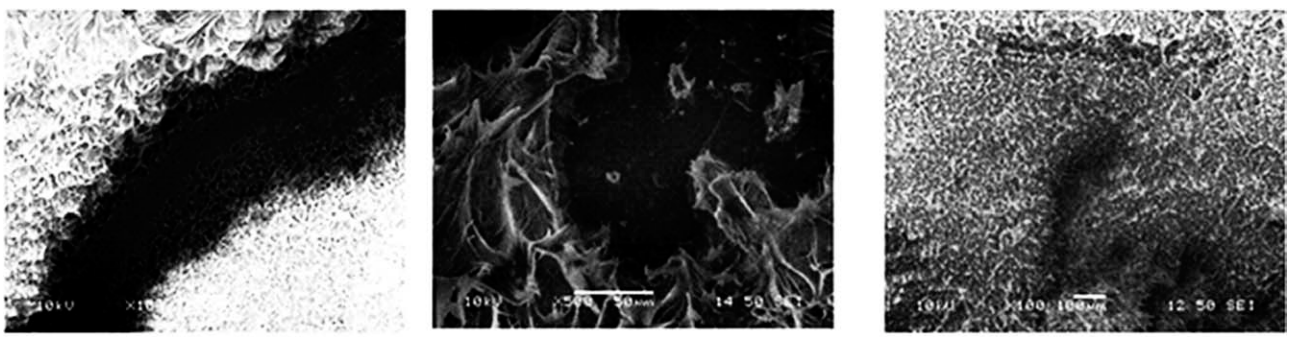

(a) (b) (c)

Figure 15 SEM micrographs of (a) NC-0, (b) NC-10, and (c) NC-20 showing induced island.

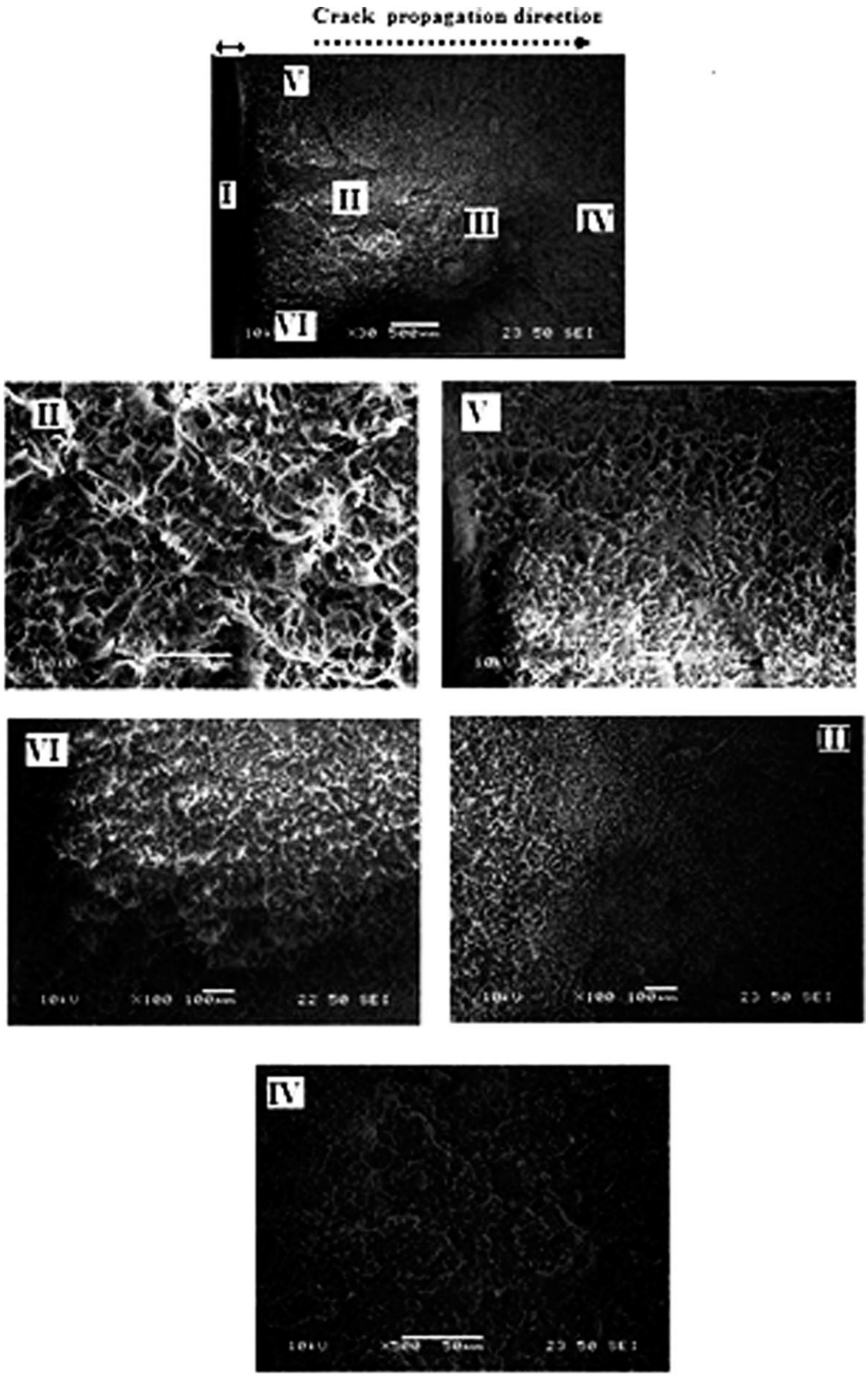

Figure 16 SEM micrographs of NC-20 showing different zones.

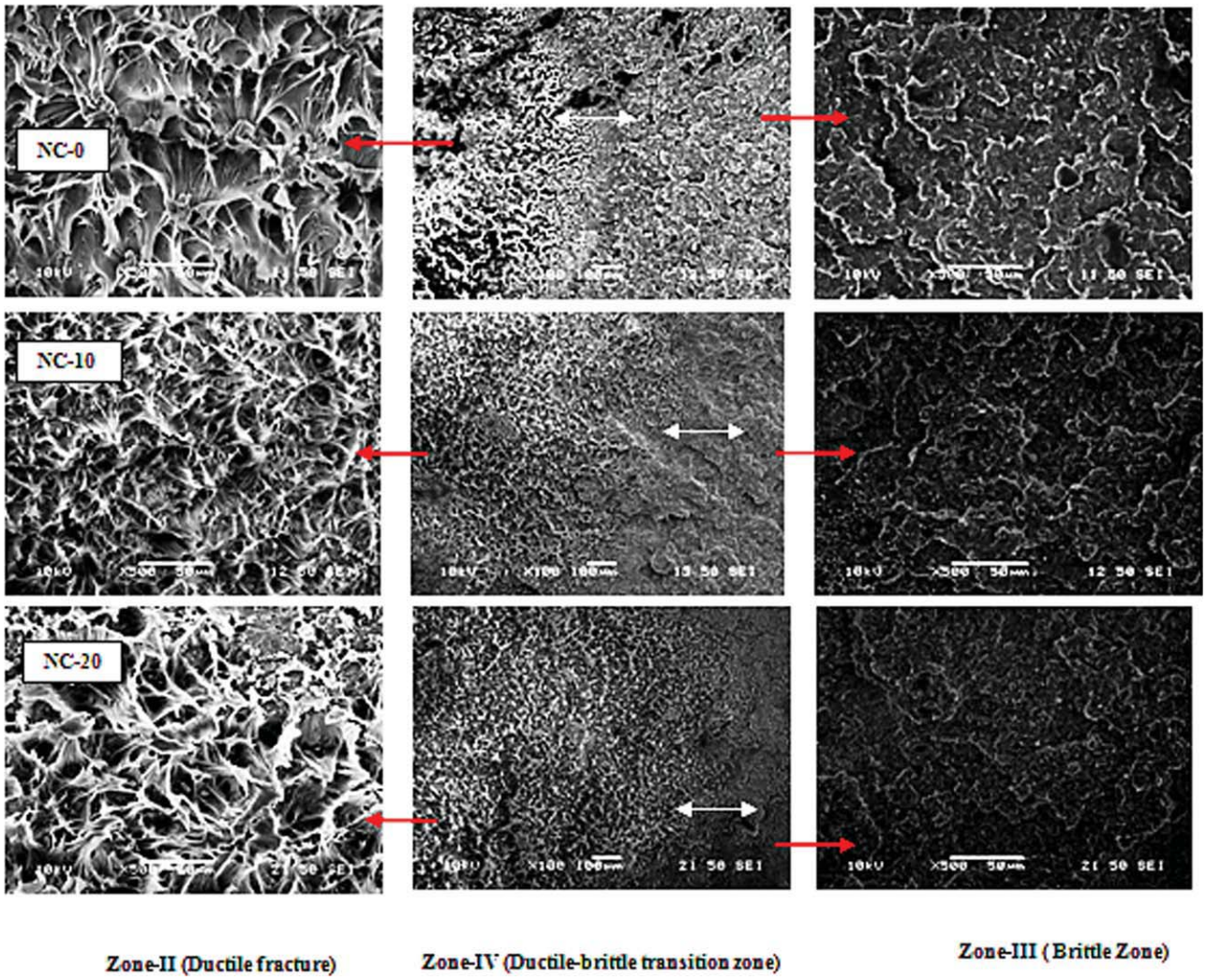

Figure 17 SEM micrographs showing ductile brittle transition zones. [Color figure can be viewed in the online issue, which is available at wileyonlinelibrary.com]

NC-0 with higher precrack-length (Fig. 15**)**. From the SEM investigations of the composite samples, it can be concluded that both precrack length and % loading dominates the fracture morphology and mechanism of fracture in these composites.

Because of the increased formation of microvoid in the interface during the fracture process in the composite samples, the fibrillation of HDPE becomes more difficult and ended prematurely as compared with neat HDPE. The formation of large number of these micro voids in the composite samples is indicative of the less ductile fracture process.[35] Overall $CaCO_3$ filled HDPE composite exhibits the fracture features of less ductile material as indicated by the debonding of $CaCO_3$ from HDPE matrix, the formation of micro voids in the interface and local plastic deformation of matrix around $CaCO_3$. This results in deterioration of the fracture toughness of composite compared with neat HDPE. Similar observations fracture features were reported by Misra et al.[42] who indicated that the main reason for such fracture characteristic was the weak interfacial interaction with the inorganic counterpart. As a stress concentrator, the nanofiller can induce the plastic deformation of around matrix, but such effect is very weak.[10,40,42] The crack propagates at a rate, which is of high magnitude such that the material does not have adequate time to respond, leading to brittle fracture Zone (IV) after the slow crack propagation Zone-II (Fig. 17).

In conclusion, the fracture toughness of a material is generally related to the energy dissipating events that occur in the vicinity of a sharp crack. In neat HDPE, the crack initiation zone is characterized by highly ductile fibrillation; while the crack initiation in calcium carbonate reinforced HDPE nanocomposites occurred by a brittle fracture mode. In the case of neat HDPE, fibrillation process releasing the plastic constraint in the matrix, triggering large scale plastic deformation with consequent extension of

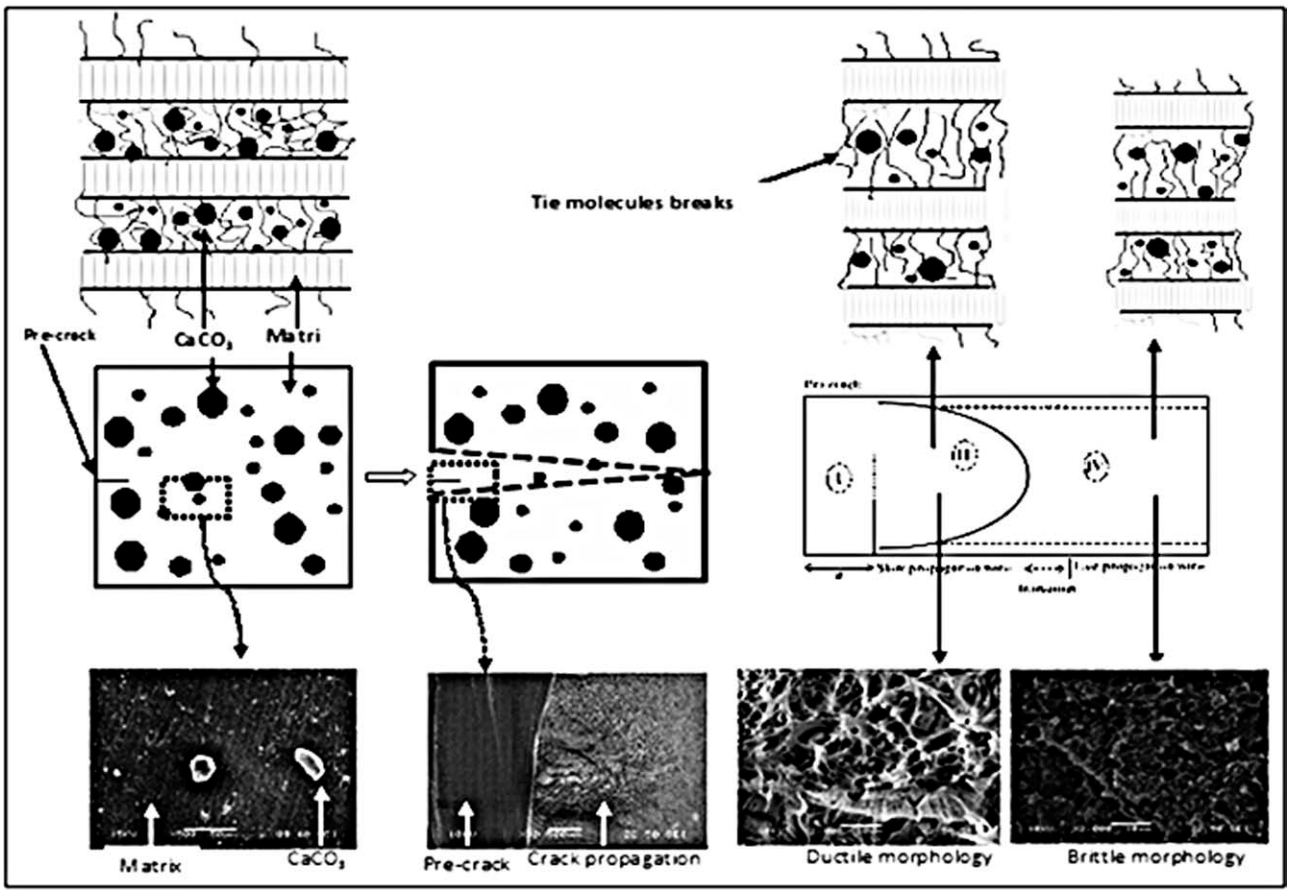

Figure 18 Schematic of the envisaged probable fracture process in HDPE/$CaCO_3$ composite.

matrix ligaments resulting in stretching of fibrils,[19,43–45] and hence slow dissipation of energy and slow crack propagation. A schematic of the envisaged fracture process in the composite samples is presented in Figure 18 describing the probable mechanism of the fracture process in the composites samples.

CONCLUSIONS

This work revealed that $CaCO_3$ content is inversely proportional to the yield strength, the fracture strain, and tensile strength. Whereas, $CaCO_3$ content is directly proportional to Young's modulus. Likewise, the testing speed is directly proportional to the tensile strength. The microscopic analysis showed that $CaCO_3$ particles debond and act as stress concentrators under applied stress. Moreover, particle interaction could generate zones of high stress that would act as areas of crack orientation. The FEM showed that elliptical particles perpendicular to stress axis are more prone to act as crack initiators than particles that are parallel to the stress axis. The fracture toughness analysis illustrated that K_I decreases as crack length increases due to the increase of stresses at the crack tip, and that K_I decreases as $CaCO_3$ percentage increases. The fractographic analysis demonstrates that ss the percentage of $CaCO_3$ increases, the dimples' length increases as well. SEN fracture surface has a mix of ductile (slow crack propagation) and brittle (fast crack propagation) features. As the crack length increases, brittle features disappeared and ductile features were dominant.

We thank SABIC Polymer Research Chair at King Saud University for providing their equipment to conduct these tests. Special thanks to Babu, Shafat, Mohammed E. Ali, and Imtiaz for conducting some of the experimental work in this research.

References

1. Dong, W. C.; Kwang, J. K.; Byoung, C. K. Polymer 2006, 47, 3609.
2. Giannelis, E. P. Adv Mater 1996, 8, 29.
3. Bhattachrya, S.; Gupta, R.; Kamal, M. R. Polymeric Nanocomposite: Theory and Practice; Hanser: Germany, 2007.
4. Steve, C.; Kurt, W. S. Prog Polym Sci 2008, 33, 797.
5. Karamipour, S.; Ebadi-Dehaghani, H.; Ashouri, D.; Mousavian, S. Polym Test 2011, 30, 110.
6. Lin, Y.; Chen, H.; Chan, C. M.; Wu, J. Macromolecules 2008, 41, 9204.
7. Xie, X. L.; Liu, Q. X.; Li, R. K. Y.; Zhou, X. P.; Zhang, Q. X.; Yu, Z. Z.; Mai, Y. W. Polymer 2004, 45, 6665.
8. Lin, Y.; Chen, H.; Chan, C. M.; Wu, J. Euro Polym J 2011, 47, 294.

9. Spitalskya, Z.; Tasisb, D.; Papagelisb, K.; Galiotis, C. Prog Polym Sci 2010, 35, 357.
10. Wang, Y.; Shi, J.; Han, L.; Xiang, F. Compos Mater Sci Eng A 2009, 501, 220.
11. Rothon, R. N. Particulate-Filled Polymer Composites. Longman Scientific and Technical: Harlow, 1995.
12. Rothon, R. N. Adv Polym Sci 1999, 139, 67.
13. Argon, A. S.; Bartczak, Z.; Cohen, R. E.; Muratoglu, O. K. In Symposium Series 759: Toughening of Plastics, Advances in Modeling and Experiments. Pearson, R. A.; Sue, H. J.; Yee, A. F., Eds.; ACS: Washington, DC, 2000; p.98.
14. Lazzeria, A.; Zebarjadb, S. M.; Pracellac, M.; Cavalierd, K.; Rosa, R. Polymer 2005, 46, 827.
15. Shah, D.; Maiti, P.; Jiang, D. D.; Batt, C. A.; Giannelis, E. P. Adv Mater 2005, 17, 525.
16. Giannelis, E. P. Toughnening of a brittle glassy polymer, poly (lactide-*co*-glycolide) by layered silicate nanoparticles (2005), Private Communication.
17. Sivaramana, P.; Chandrasekhara, L.; Mishraa, V. S.; Chakrabortya, B. C.; Vargheseb, T. O. Polym Test 2006, 25, 562.
18. Liu, L.; Yong, W.; Yanli, L.; Jun, W.; Zuowan, Z.; Chongxi, J. Polymer 2009, 50, 3072.
19. Bartczak, Z.; Argona, A. S.; Cohena, R. E.; Weinberg, M. Polymer 1999, 40, 2331.
20. Fu, S. Y.; Lauke, B. J Mater Sci Technol 1997, 13, 389.
21. Fu, S. Y.; Lauke, B. Composite 1998, 29A, 631.
22. Baker, R. A.; Koller, L. L.; Kummer, P. E. In Handbook of Fillers for Plastics, 2nd ed.; Katz, H. S.; Milevski, J. L., Eds.; New York: Van Nostrand Reinhold Co, 1987; p 119.
23. Fu, Q.; Wang, G. Polym Eng Sci 1992, 32, 94.
24. Fu, Q.; Wang, G.; Shen, J. J Appl Polym Sci 1993, 49, 673.
25. Fu, Q.; Wang, G. J Appl Polym Sci 1993, 49 1985.
26. Fu, Q.; Wang, G. Polym Int 2007, 30, 309.
27. Bartczak, Z.; Argon, A. S.; Cohen, R. E.; Weinberg, M. Polymer 1999, 40, 2347.
28. Lazzeri, A.; Zebarjad, S. M.; Pracella, M.; Cavalier, K.; Rosa, R. Polymer 2005, 46, 827.
29. Lee, S. H.; Kim, M.; Kim, W.; You, S. H. Eur Polym J 2008, 44, 1620.
30. Potschke, P.; Fornes, T. D.; Paul, D. R. Polymer 2002, 43, 3247.
31. Elleithy, R. H.; Ali, I.; Ali, M. A.; Al-Zahrani, S. M. J Appl Polym Sci 2010, 117, 2413.
32. Elleithy, R. H.; Ali, I.; Ali, M. A.; Al-Zahrani, S. M. J Reinforced Plast Comp, DOI: 10.1177/0731684411400111.
33. Liu, Z. H.; Zhu, X. G.; Li, Q.; Qi, Z. N.; Wang, F. S. Composites 1998, 39, 1863.
34. Zebarjad, S. M.; Sajjadi, S. A. Mater Sci Eng A 2008, 475, 365.
35. Williams, J. G. Fracture Mechanism of Polymers; Ellis: Horwood, 1987.
36. Sahebian, S.; Zebarjad, S. M.; Sajjadi, S. A.; Sherafat, Z.; Lazzeri, A. J Appl Polym Sci 2007, 104, 3688.
37. Hornsby, P. R. Adv Polym Sci 1999, 139, 155.
38. Lauke, B. Comps Sci Technol 2008, 68, 3365.
39. Fu, S. Y.; Feng, X. Q.; Lauke, B.; Mai, Y. W. Composites: Part B 2008, 39, 933.
40. Deshmane, C.; Yuan, Q.; Misra, R. D. K. Mater Sci Engg A 2007, 453, 592.
41. Cotterell, B.; Chia, J. Y. H.; Hbaieb, K. Eng Fracture Mech 2007, 74, 1054.
42. Li, B.; Gong, G.; Xie, B. H.; Yang, W.; Yang, M. B. J Appl Polym Sci 2008, 109, 1161.
43. Yuan, Q.; Misra, R. D. K. Polymer 2006, 47, 4421.
44. Kwon, S.; Kim, K. J.; Kim, H.; Kundu, P. P.; Kim, T. J.; Lee, Y. K.; Lee, B. H.; Choe, S. Polymer 2002, 43, 6901.
45. Rattanawijan, W.; Amornsakchai, T.; Amornsakchai, P.; Petiraksakul, P. J Appl Polym Sci 2009, 113, 1887.